THE JOURNAL OF PHYSICAL CHEMISTRY C

Subscriber access provided by Universitaetsbibliothek | Johann Christian Senckenberg

Article

On the Radiation Damage Mechanisms of Monolayer-protected Nanoparticles via TEM Analysis

Julio César Azcárate, Mariano Hernán Fonticelli, and Eugenia Zelaya

J. Phys. Chem. C, **Just Accepted Manuscript** • DOI: 10.1021/acs.jpcc.7b08525 • Publication Date (Web): 19 Oct 2017

Downloaded from http://pubs.acs.org on October 20, 2017

Just Accepted

“Just Accepted” manuscripts have been peer-reviewed and accepted for publication. They are posted online prior to technical editing, formatting for publication and author proofing. The American Chemical Society provides “Just Accepted” as a free service to the research community to expedite the dissemination of scientific material as soon as possible after acceptance. “Just Accepted” manuscripts appear in full in PDF format accompanied by an HTML abstract. “Just Accepted” manuscripts have been fully peer reviewed, but should not be considered the official version of record. They are accessible to all readers and citable by the Digital Object Identifier (DOI®). “Just Accepted” is an optional service offered to authors. Therefore, the “Just Accepted” Web site may not include all articles that will be published in the journal. After a manuscript is technically edited and formatted, it will be removed from the “Just Accepted” Web site and published as an ASAP article. Note that technical editing may introduce minor changes to the manuscript text and/or graphics which could affect content, and all legal disclaimers and ethical guidelines that apply to the journal pertain. ACS cannot be held responsible for errors or consequences arising from the use of information contained in these “Just Accepted” manuscripts.

ACS Publications

The Journal of Physical Chemistry C is published by the American Chemical Society.
1155 Sixteenth Street N.W., Washington, DC 20036

Published by American Chemical Society. Copyright © American Chemical Society. However, no copyright claim is made to original U.S. Government works, or works produced by employees of any Commonwealth realm Crown government in the course of their duties.

On the Radiation Damage Mechanisms of Monolayer-protected Nanoparticles via TEM Analysis

Julio C. Azcárate[†], Mariano H. Fonticelli[‡], Eugenia Zelaya[†]*

† Centro Atómico Bariloche (CAB), CONICET, Av. Bustillo 9500, San Carlos de Bariloche, Argentina.

‡ Instituto de Investigaciones Fisicoquímicas Teóricas y Aplicadas (INIFTA), UNLP, CONICET, Calle 64 y diag. 113, La Plata, Argentina.

ABSTRACT

In this work it is shown that thiol-protected Au nanoparticles (AuNPs@SR) of approximately 3.4 nm in size suffered unexpectedly high radiation damage under standard transmission electron microscopy (TEM) operating conditions. For metallic systems (conducting sample) it is expected that the greatest contribution to the damage to come from knock-on displacement, but radiolysis is the most probable radiation damage mechanism for organic samples. The radiation damage of the electron beam produce huge changes in AuNPs' structure, leading to coalescence of the Au cores when their {100} surface are facing each other. The complete coalescence process involve thiol desoprtion, AuNPs' reorientation and surface diffusion of Au adatoms, which produce the oriented attachment of the Au cores. The knock-on displacement cannot explain by itself the time taken by the entire process. Through a rigorous analysis we rationalize the results

considering that because of the small size of AuNPs they have a lower electron density than the bulk material, which favors radiolytic damage.

Introduction

Most of the advanced analytical techniques involve some kind of radiation (photons or electrons are the most popular) to analyze the sample. It is well known that the interaction between radiation and matter can cause sample damage, which must be thoughtfully characterized and taken into account for correct data interpretation.

Transmission electron microscopy (TEM) is an advanced technique where electrons are accelerated up to energies of hundreds of keV across the sample to obtain structural information. In materials science, TEM has huge importance and the radiation damage it produces has been extensively studied for bulk materials. Nevertheless, the radiation damage in new materials like those based on nanoparticles is less explored.

Nanoparticles (NPs) acquired great interest in the last few years and many novel applications are based on them. Thiol capped gold NPs (AuNPs@SR) are one of the most studied NPs and they are considered a model systems when compared with those constituted of other metals. AuNPs@SR can be synthetized by several methods depending of the nature of the thiols. The two-phase approach by Brust and Schiffrin[1] is extensively used because it allows excellent size control by tuning the thiol/metal ratio. It leads to narrow size distributions for NPs < 6 nm.[2] However, some fundamental features like chemical composition and structure are not completely described or known. Moreover, the analysis of composition, size and structure performed by different and complementary techniques do not always lead to compatible results.[3,4] In those cases it is of paramount importance the understanding and quantification of radiation-damage processes.[5,6]

The AuNPs@SR present the fcc structure of Au, however they change their shape according to their size. Different geometries for AuNPs were widely reported in literature.[7–11] Figure 1 shows the most commonly observed shapes in the present work: a truncated octahedron (a) and a truncated decahedron (Marks Decahedron) (b and c). These geometries are described for bare (uncapped) or weak-ligand capped NPs. The truncated octahedron (Figure 1a and 1d) is the most stable geometry according to thermodynamic arguments,[9] and their faces are crystalline planes of the {111} and {100} families of an fcc structure. The case of the truncated decahedron described by Marks corresponds to pentagonally twinned NP, with plane faces exposing the above mentioned families of planes ({111} and {100}). Nevertheless, it is well know that thiols alter the surface structure of NPs due to their strong covalent bonds with metallic atoms.[6,12] Figures 1d-f show HRTEM images of AuNPs@SR with shapes similar to the above models near the [011] axis zone (Figures 1a-c). Here, a projection of the {111} and the {100} surfaces along the [011] axis zone can be observed.

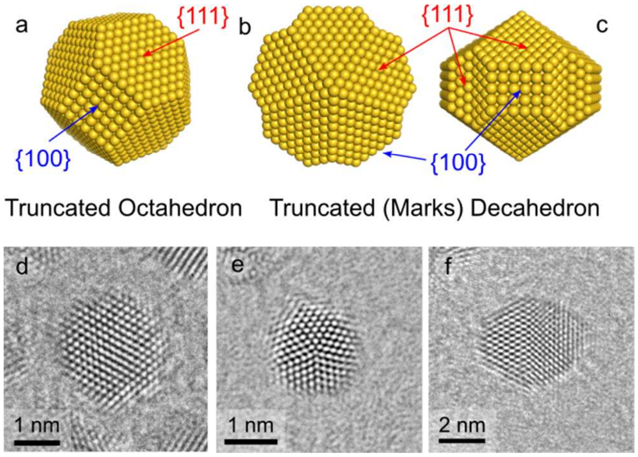

Figure 1: Sphere-models representation of (a) a Truncate Octahedron and (b-c) of a Truncated (Marks) Decahedron. (d-f) Representative examples of AuNPs@SR imaged in HRTEM mode.

It is well known that electron radiation causes damage on samples during a TEM session.[13] The radiation damage may have different origins depending on the nature of the samples and the operation parameters. The radiation damage was widely studied for bulk materials like metals (conducting), semiconductors, and inorganic solids or polymers (insulators). Electron radiation damage acts by several mechanisms depending on the scattering type: *Elastic* or *Inelastic*. Elastic scattering occurs by electrostatic deflection of the electron beam due to the Coulomb field of the atomic nuclei. This scattering gives electron-diffraction patterns and phase contrast in TEM images. In both cases, the elastic scattering leds to the so-called knock-on displacement, producing changes in the atomic positions or sputtering of the surface atoms. On the other side, inelastic scattering occurs by the Coulomb interaction between the electron beam and the atomic electrons of the sample. This scattering induces electronic excitation which produces secondary-electrons, emission of X-rays, and can also be responsible for radiolysis effects or heating.[14] There are several papers on radiation damage of particles since the 80's decade to these days, but most of them were performed on bare NPs[15–18] instead of capped NPs[19,20]. However, the radiation damage mechanism was not explored in detail. For this reason, it is paramount to deeply study the consequences of electron irradiation damage on capped-NPs.

The aim of this paper is the characterization and analysis of the main sources of radiation damage over AuNPs@SR during TEM imaging. The changes that NPs suffered were recorded in HRTEM images over time. First, we described the observed AuNPs coalescence induced by electron beam irradiation during HRTEM imaging. Thus, a careful HRTEM analysis under different operation condition (varying exposure doses) have shown that two AuNPs coalesce only when the {100} planes face each other (oriented attachment). This interesting result was confirmed for representative pairs of nanoparticles' geometries (two truncated octahedrons, truncated octahedron and Marks' decahedron, and two Marks' decahedrons). Then, the different causes of damage –knock-on, radiolysis and thermal heating– were considered and the effect they can have on AuNPs@SR was estimated. We concluded that the main cause of radiation damage is attributed to radiolysis process, which cannot be avoided in HRTEM mode at room temperature. In this operation mode the radiation damage can drastically alter the sample, leading to AuNPs@SR coalescence.

Experimental

Synthesis of AuNPs@SR: the nanoparticles were prepared using the two liquid phases method developed by Brust and Schiffrin.[1] First, 137 mg of tetraocthylamonium bromide, TOABr (Sigma-Aldrich) were dissolved in 8 mL of toluene (Carlo Erba) in a round bottom flask. Then, 4 mL of $HAuCl_4$ 25 mM solution (0.1mmol of Au) in HCl 100 mM were added and the mixture was stirred until the complete transfer of $AuCl_4^-$ to the toluene phase. The aqueous phase was removed and the toluene solution was washed once with 5 ml of H_2O to remove the acid excess. Afterwards, under constant stir, 9 µL of dodecanethiol (Sigma-Aldrich) were added to the mixture. After 10 minutes, 38 mg of $NaBH_4$ in 3 mL of H_2O were added quickly. The stir was kept for 3 hs to promote a narrow size distribution. Both phases were separated, and toluene was evaporated keeping a tenth of this liquid phase. AuNPs were purified by precipitation with 15 mL of ethanol, and were centrifuged after 30 min. This purification procedure was repeated three times.[21] Then, the AuNPs were dried and stored as powder at -18ºC.

Specimen preparation: the AuNPs were redispersed in toluene and then drop-casted on 300 mesh ultrathin carbon film on holey carbon support copper grids.

TEM imaging and data analysis: Two transmission electron microscopes were used to carry out the radiation damage studies: a Phillips CM200 UltraTwin (LaB_6) and a FEI Tecnai F20 G2 (FEG), both operated at 200 keV. The current measurements were developed using a Gatan 646 Double Tilt Analytical Holder connected to a Keithley 6485 Picoammeter.

HRTEM images simulation were carried out with JEMS software.[22] The proper orientation of atomic models of NPs for simulation were made using a software developed in the physics of metals division at Centro Atómico Bariloche.[23]

Results and Discussion

At the start of the TEM observation, the bright field images of the sample revealed the presence of NPs spread across the entire carbon film. However, after some minutes of observation of the same area, a coalescence of particles can be obtained. The figure 2 shows the difference between the fresh sample and the particles observed by HRTEM after a few minutes. The particles viewed at first time were round and homogeneously dispersed, as can be seen outside the green coloured area. The particles observed in HRTEM mode or bright field condition presented the same characteristics at the green colored area. However, they look rather bigger than at the beginning and not as rounded as the particles viewed for the first time. The size distribution was obtained from images taken at the same magnification of not irradiated areas; it was fitted with a lognormal function resulting in a mean diameter of 3.4 nm ± 0.8 nm (see Supplementary Information).

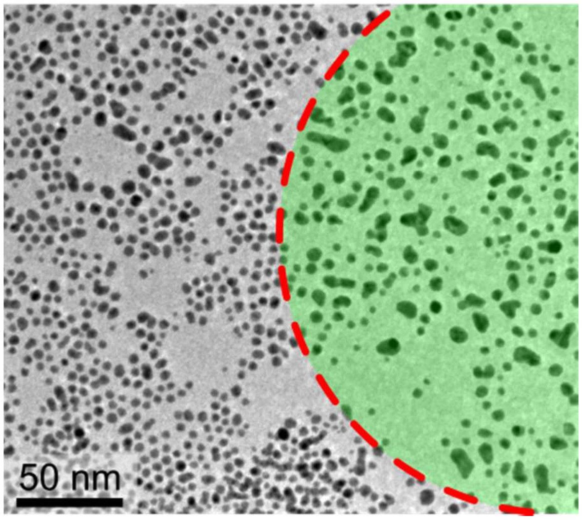

Figure 2: Bright field image of AuNPs@SC12. The green marked zone was previously observed in HRTEM condition. The image is slightly underfocus to reinforce the contrast.

Next, it will be shown that the electron beam induces coalescence and ripening processes. Because most of the nanoparticles were found to be truncated octahedrons and truncated (Marks) decahedrons, in what follows we present studies of radiation damage for both kind of nanoparticle shapes. The first pair of particles were two truncated octahedrons (Figure 3). The nanoparticles are expected to be randomly oriented before their irradiation. However, most of the particles are preferentially oriented along a low-index zone axis.

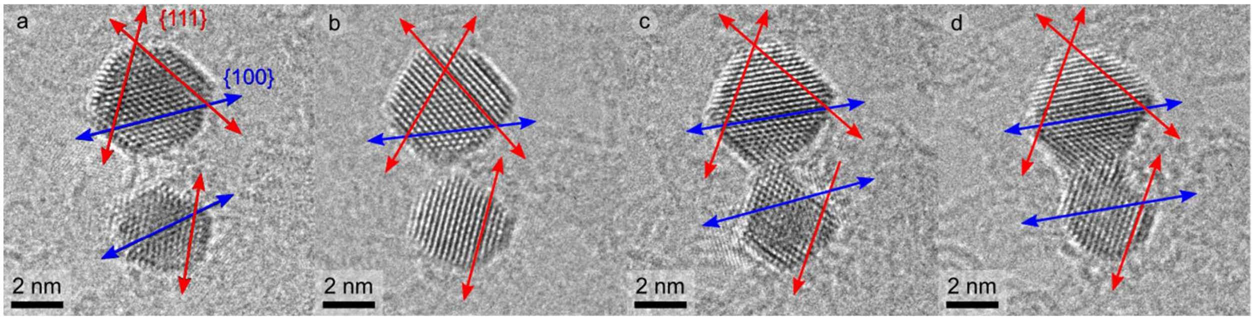

Figure 3: Coalescence of tow truncated octahedron like AuNPs. Red arrows represent the planes type {111} and the blue ones {100} along the [011] zone axis. The images were taken at: a) 1037 s, b) 1097 s, c) 1158 s and d) 1195 s after start irradiation.

Figure 3 shows the coalescence of two truncated octahedrons when {100} planes of each particle are facing to each other. In the beginning -Figure 3a and Figure 3b-, the planes {111} and {100} from one particle are not aligned with the same family of planes of the other. In Figure 3c the {100} faces of each octahedron are close to be parallel. At this point, the shape of the octahedron at the bottom of this panel starts to change. It seems that few Au atoms form a column between the two AuNPs. Moreover, there is no evidence of boundaries between the particles. This HRTEM image was simulated to corroborate that both AuNPs are at the same height with both planes {100} facing each other (see Supplementary Information). Finally, in

Figure 3d it could be distinguished a unique orientation for the {111} and the {100} families of planes. Furthermore, the evolution of the two octahedron system continued until the formation of a unique faceted NP was reached. This coalescence process where two particles joint to form a new bigger one is also called *Smoluchowski ripening.*[24] An increase in the roughness of the amorphous carbon substrate is also evident which a consequence of electron beam radiation damage is.

It is worth to mention at this point that the coalescence seems to be reached after the reorientation of the {111} and {100} planes of the NPs, which is attributed to an “electron wind”.[25] This reorientation is evident in the smaller nanoparticles. Even more, the nanoparticles' displacements can be as large as their sizes. However, this pivot is not observed in the bigger NPs due to their higher masses (moment of inertia).

At this point, the coalescence observed looks similar to the previously reported on bare AuNPs,[17,18] but in this case the AuNPs are capped by an alkanethiolate monolayer. The first question is: RS monolayer is still on AuNPs? In order to describe the coalescence of two particles of similar sizes, two scenarios are considered. In the simplest reasoning, the particles coalesce when their naked surfaces encounter. Previously, the radiation damage must have stripped-off the RS moieties at least from the {100} faces. In a more complex reasoning, if the capping-agent were still on the {100} faces that stick each other the adsorbates should leave both faces within about a minute while coalescing (Figures 3c-d, 4d-e and 5b-g). In other words, a concerted movement of the RS species should occur, in order to lead to a single fcc structure like the ones observed in the figures 3d, 4e and 5g. Furthermore, this concerted mechanism could also be done across {111} faces and not only across {100} faces. But coalescence was not observed across {111} (see below). On the other hand, as the total metallic core surface decrease due to the coalescence, the RS moieties could not simply rearrange over the new formed particle because their coverage would increase. However, when the size increases the coverage decreases[2,26] to the same value as the self-assembled monolayer on flat surfaces.[26] In a simple calculation, two nanoparticles of similar sizes than those shown in Figure 3 are formed by 976 Au atoms and 187 RS chains (3 nm) and 314 Au atoms and 91 RS chains (2nm), respectively.[2] The coalescence of these AuNP@RS would lead a bigger one of 1290 Au atoms and 221 RS chains (3.2 nm)[2]. However, the sum of RS chains of both individual AuNP@RS are higher than the expected (57 RS chains in excess). Also for this reason, the second mechanism does not seem to be probable.

It is clear that at least the {100} faces must be free of adsorbed molecules (uncapped or bare). Otherwise, the coalescence process shown in Figure 3 would not occur. Notably, it was reported that the coalescence processes of two naked NPs is a spontaneous and non-activated processes.[19]

The electron radiation damage could produce the total or partial desorption of the adsorbed thiols. However, it is not clear up to now whether the adsorbates leave the surface as thiolate, thiyl, radical fragments and/or some of the reported staples.[3,27] After thiol desorption, the exposed metallic surface of a NP can get in contact with the bare surface of a surrounding NP, thus producing their coalescence.

It is commonly believed that the increase in temperature is responsible for the adsorbate desorption. However, the electron beam heating is overestimated,[7] and the calculation of the temperature rise shows an increase of less than 2 K in AuNPs smaller than 10 nm (See Supplementary Information for details in calculation).

As a second case study, Figure 4 shows the coalescence of a twinned truncated (I) octahedron and a truncated decahedron (II) AuNPs. Once again, the coalescence process starts just when the {100} faces of both NPs are facing each other (Figure 4e). The black arrows (Figure 4b) are showing the stacking fault planes where the {111} and {100} planes are in similar directions. It is interesting to note that the atomic planes rearrange, so that the stacking fault vanishes. Only when it seems to disappear, the coalescence between both AuNPs starts. It is noticeable that just before coalescence, Figure 4d, the truncated octahedral NP (I) does not expose a complete {100} surface to the other NP. This observation suggests that coalescence occurs when equal planes are facing each other. Even more, this result suggests that if the existence of a defect avoids the facing of the {100} faces, the coalescence would not occur until the defect disappears.

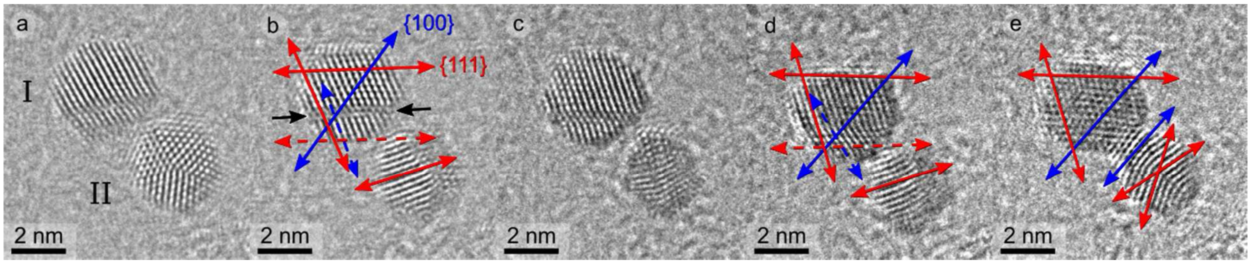

Figure 4: Coalescence of a twinned truncated octahedron (I) and a truncated decahedron (II). The images were taken at: a) 346 s, b) 390 s, c) 463 s, d) 498 s and e) 553 s after start irradiation. The red arrows indicate the planes {111} and the blue ones {100} planes along the [011] zone axis. Black arrows show the stacking fault plane, and the dashed arrows show planes in the other side of this plane.

The last processes to be illustrated involve two pairs of truncated (Marks) decahedrons (Figure 5). These AuNPs were all together in the same region and received exactly the same radiation dose. The two particles in the top-panels (Figure 5 a-g) show, once again, the coalescence through the {100} faces of both AuNPs. In the other case (Figure 5 h-n), the bottom AuNP reduces its size over time until it disappears. This mechanism was reported and described as an Ostwald ripening process, which was previously observed by STEM.[19] On the contrary, the particles bigger than ~2nm seem to coalesce when the {100} faces encounter. The Ostwald ripening occur by unbalanced atomic diffusion from the smaller NPs to the bigger one. On the basis of computer simulations it was proposed that Ostwald ripening can be induced by electronic irradiation occur without thiol desorption.[19] However, the system could be trapped on local energy minimum, which could impede the full Ostwald ripening process. Also, the Ostwald ripening on a totally naked AuNP is not favored.[19] Nevertheless, the presented results suggest that the ripening is favored when the {100} faces are naked. In all cases, after coalescence, the new formed particle suffer a rearrangement of their atoms to get a shape with a lower surface energy. This is evident in the Figure 5e-g, where the arrows indicate the vertex changes on the bigger (up-left) particle. This kind of rearrangement of the surface atoms was reported for different metallic NPs.[28,29]

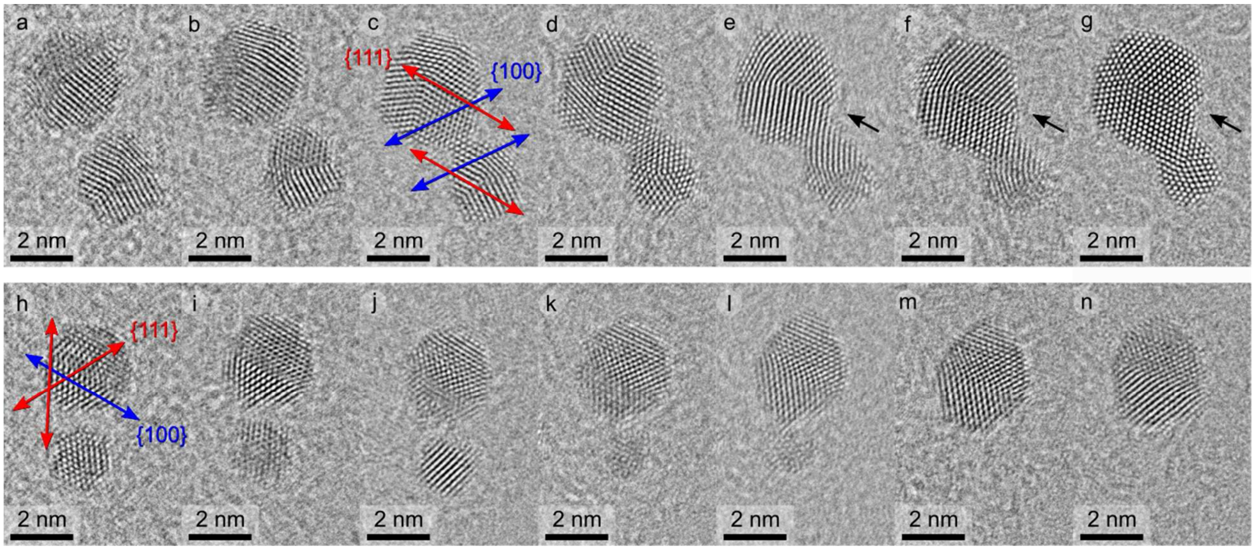

Figure 5: Four truncated (Marks) decahedron suffering coalescence (a-g) and ripening (h-n). These AuNPs were nearby and consequently exposed to the same radiation doses. The AuNPs

are near to the [011] zone axis. The images were taken at: (a;h)=110 s, (b;i)=170 s, (c;j)=274 s, (d;k)=361 s, (e;l)=385 s, (f;m)=460 s and (g;n)= 485 s.

Noticeably, no coalescence nor ripening events were observed between surfaces that exposed planes different from the {100}, even when two nearby NPs rotate (or pivot) during a long time (see Supplementary Information, Figure SI 3). In these cases, it is observed that nanoparticles' crystalline planes are not aligned. Moreover, both coalescence processes do not depend on the received doses, but on nanoparticles' orientation: the most important factor in coalescence phenomena here described is the parallel alignment of the {100} faces.

All these results suggest that at least the {100} faces are uncovered by thiols when the coalescence occurred. This can be explained considering that radiation damage can induce thiol desorption. Indeed, migration of Au atoms and Au-SR moieties were reported for the case of ripening.[19] In this direction it is proper to analyze the possible mechanisms of radiation damage involved in the capping degradation.

Analysis of Mechanism Involved in Radiation Damage

After discarding the temperature increase as a significant source of sample damage, two main mechanisms involved in this kind of radiation damage still remains: Knock-On displacement (by elastic scattering) and Radiolysis (by inelastic scattering). Knock-On displacement involves the energy transfer during elastic scattering between the incoming electron and the atomic nucleus of the sample. The energy transferred could displace the atom away from their natural vibrational position, giving the breakdown of several chemical bonds. The term "radiolysis" involves several chemical changes induced by inelastic interaction between the incoming electrons with the atomic electrons in the sample. The inelastic scattering produce electronic excitation or ionization which could relax by several ways (e.g. chemical bonds scission). The chemical bonds scission implies atomic displacements. The necessary conditions for this atomic displacements are localization of an electronic excitation with sufficient energy and for sufficiently long times (longer than the time for an atomic vibration, or ~l ps). That mechanical relaxation of the surrounding atomic cores leads to a bonding instability, in many cases involving displacement of atomic cores. In this way the potential energy inherent in electronic excitations can be converted to momentum of a departing atom nucleus.[30] For conducting materials, like metals, the electrons in their conductive bands compensate extremely fast (~1fs) the ionization processes or collective electronic excitation (plasmonic excitation) decreasing the radiolysis effects.[30] However, in non-conductive materials, like organic materials, the charge reposition is not so fast to avoid chemical scission due to electronic rearrangements of excitation or ionization. The nanoparticles studied here should not be considered a priori nor as a typical conducting materials nor as an insulator. Then, it is necessary to evaluate and compare both mechanisms to determine which one is the most important. This could help to establish possible strategies to avoid or diminish the TEM radiation damage. Egerton reported in several articles and reviews about TEM and SEM radiation damage.[14,31,32] Cross-section values (σ) or critical doses (De) were determined for different bulk materials. In the next paragraphs, both mechanisms are described and compared.

First, we analyzed the atomic displacement produced by elastic scattering, which can occur in all kind of samples but is evident in crystalline specimens (blurring the electron diffraction pattern). In order to estimate the cross sections for knock-on events, σ_d, we will start focusing on a few relevant magnitudes: the energy of the incident electrons, E_0, the maximum energy transferred by knock-on impact of an incoming electron, E_{max}, and the energy needed to get an atomic displacement, E_d. When $E_{max} < E_d$, displacement damage is absent since the incident energy is bellow certain threshold incident energy (E_0^{th}). E_0^{th} is above 200 keV for most of the elemental solids, but its value is considerably lower for organic materials (lighter elements). According to Egerton *et al*. E_{max}, is given by[31]:

$$E_{max} = \frac{E_0(E_0 + 2m_0c^2)}{\left[E_0 + \left(1 + \frac{m_0}{M}\right)^2 \frac{Mc^2}{2}\right]} \approx \frac{2E_0(E_0 + 2m_0c^2)}{Mc^2}$$

where m_0 is the electron rest mass, c is the speed of light and M is the mass of the knocked atom. Note that the energy transferred rises as the energy of the incident electrons increases, and it is larger for lighter elements. On the other hand, the displacement energy, E_d, strongly depends on the strength and number of bonds in which the specific atom participate. In the case of small NPs most of the atoms are on the surface. For this reason, it is proper to consider that sputtering displacement is more important than “bulk” knock-on damage. Thus, the AuNPs@SC12’ surface chemistry might be considered in some detail in order to get reliable results. Another drawback comes from the fact that displacement energies E_d are not well known for organic molecules. Nevertheless, an estimation of the total atom bond energy can be used instead E_d as good approximation.[32] Two models of thiol adsorption has been reported: on bridge “standard” site and staple motif. Recently, it was proposed that thiols adsorb as thiyl moieties rather than thiolate moieties.[33] Henceforth, the RS moieties represent either kind of chemical species, thyil or thiolate. In the standard model, the sulfur atom is bonded on bridge sites of a perfect Au(hkl) surfaces.[33–35] In the staple motif model two RS moieties are bonded to an Au adatom, and also to the Au surface atoms (Au-RS-Au_{ad}-RS-Au).[33–35] For the Au(111) surface the energy per RS unit is lower in the staple configuration than for the bridge site. Notably, the opposite was reported for Au(100), being the adsorption on the bridge site more favorable than on a staple motif.[35] In our calculation we have chosen the adsorption energy that corresponds to the less stable RS moiety (i.e RS in a bridge site of an Au(111) surface; adsorption energy of -1.5 eV)[33], which is equivalent to the greater knock-on cross-section (see below). The energy for Au on Au(111) surface is -3.44 eV and for Au on borders is -3.12 eV.[34] The bond dissociation energy of the relevant covalent bonds are: C-H 4.2 eV; C-C 3.7 eV and C-S 3.2 eV (as an approximation, it is considered that these energies are the same than those on an alkanethiol molecule).[36] As an example for AuNPs@SC12 consider that a sulfur atom is displaced when two bonds are broken: one between sulfur and the alkyl carbon (S-C) and the other between sulfur and gold (Au-S), taking into account the different models on RS adsorption. The energy E_d is the sum of every broken bond. The atom displaced is bold labelled in Table 1 and Figure 6. Table 1 shows the E_d values considered in each displacement case. These estimated values for E_d can be used to calculate the cross section for knock-on, σ_d, displacement as: [32]

$$\sigma_d = (0.25\text{barn})F(\upsilon)Z^2\left[\frac{E_{max}}{E_d} - 1\right]$$

where $F(\upsilon) = \gamma^{-2}(\upsilon/c)^{-4} = (1-\upsilon^2/c^2)(\upsilon/c)^{-4}$, and Z is the atomic number of the displaced atom. Clearly, the probability to get an atomic displacement increases with the atomic number, but decreases with the atomic mass. Then, the mean time between damage events (τ) could be estimated from:

$$\tau = \frac{1}{J\sigma_d}$$

where J is the electron flux. Figure 6 shows the variation of the atomic displacement cross section as a function of the energy of the incident beam. The most probable displacement by knock-on at 200 keV acceleration voltage corresponds to the sulfur atom (Au-**S**-chain). Note that for this electron-acceleration it is infrequent to displace gold atoms off the metallic surface (Au-**Au$_s$**-S). Thus, the reduction of the acceleration voltage, a standard strategy to reduce the knock-on damage, would have negligible effect in the Au atoms displacement. In addition, the displacement of total thiol molecule was considered (Au-**S-chain**), but its cross-section is smaller than that of amorphous carbon. All in all, the time required for each damage event is very long. While on average it takes ~17 min to displace a sulfur atom by knock-on (Table 1), the time required to observe coalescence, which necessarily implies many damage events, was shorter than this figure (10^2 s). Moreover, as a direct comparison between theoretical and experimental data could not be straightforward, we also considered a lower E_d (higher cross section) for Au-**S**-C knock-on displacement. If one half of the previously used E_d was taken (i.e E_d =2.4 eV for Au-**S**-C) the time per each damage event will be ~8 minutes. Then, the S displacement by knock-on should not be considered as the main source of radiation damage. In the same way, the knock-on displacement cannot explain the migration of Au atoms or Au-SR moieties between NPs necessary for the *Ostwald Ripening* process.[19] In figure 6 the knock-on cross section curves for Au atoms on borders and Au-SR moieties (orange and green dashed lines, respectively) show that they would only be displaced if the energy of the incoming electrons is bigger than 200 keV.

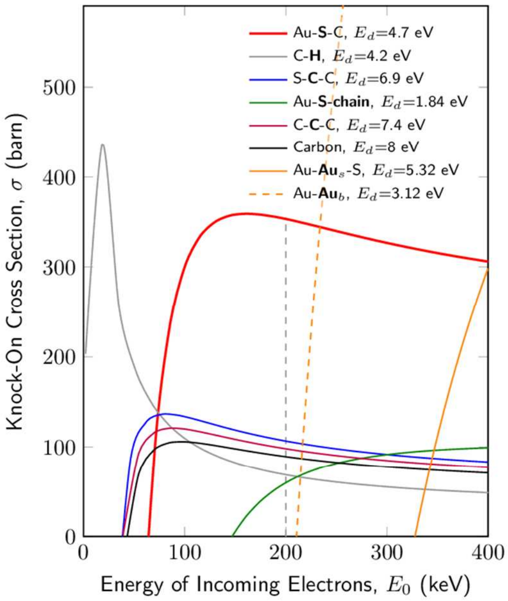

Figure 6: Knock-On cross section for atomic displacements of different atoms and molecular moieties on alkanethiol protected gold nanoparticles.

Table 1: Bond types and cross sections for knock-on and radiolysis as mechanisms of radiation damage. Accelerating voltage = 200 keV, ***J***= 2.8×10^{18} e·s^{-1}·cm^{-2}.

Bond	**Ed (eV)**	**σd (barn)**	***τ* (s)**	**Mechanism**
		Nanoparticles[34]		
Au-**Au$_s$**-S	5.32	-	-	**Knock-On**
Au-**S**-C	4.7 (~2.4)[a]	355 789	1006 453	**Knock-On**
Au-**S-chain**	1.84	59	6053	**Knock-On**
S-**C**-C	7	105	3401	**Knock-On**
C-**C**-C	7.4	98	3644	**Knock-On**
C-**H**	4.2	60	5952	**Knock-On**
		Bulk Mat.[31]		
Carbon film	8	89	4013	**Knock-On**
Organic		10^5-10^8	4–0.004	**Radiolysis**
Inorganic		0.1-10^6	40000–0.4	**Radiolysis**
Conducting	10-50	10^2-10^3	4000-400	**Sputtering**

[a] sub-estimation of the E_d value considering the half of the calculated value for both bonds scission.

The last radiation damage mechanism to be studied is radiolysis, which is associated with inelastic scattering. The energy loss of the incoming electrons can produce electronic transitions in the sample. One of the effects of these electronic transitions is to drive chemical reactions between organic or inorganic species. Radiolysis is, in general, less important in conducting materials like metals. For the sake of comparison, Table 1 presents the displacement energy, E_d, cross section and the involved mechanism in alkanethiol capped gold nanoparticles. The range of values for radiolysis cross sections reported in the literature for organic or inorganic bulk samples is also shown.

Thiol capped nanoparticles could not be classified as typical organic, inorganic or metallic materials. They are not conducting materials -as bulk metals are- and could be similar to either organic molecules or inorganic materials. Furthermore, the smaller NPs have discrete electronic levels similar to molecules.[27] Whatever the chemical nature chosen for the comparison was, the time-scale of the radiolysis events is by far smaller than those estimated for knock-on displacements. Moreover, considering that radiolysis causes electronic excitation in the sample, it is expected that the frontier molecular orbitals close to the sulfur atom were affected. Then, it is reasonable to hypothesize that RS units and/or Au_s-S-chain units would detach from the NPs' surface before the coalescence or ripening processes starts. Scheme 1, panel A, represents the RS desorption due to radiolysis. The thiol desorption is a necessary but not sufficient condition for the coalescence of the nanoparticles. According to our experimental findings the particles coalesce only when two RS free {100} faces encounter (Scheme 1, panel B). This can be explained considering that the electron flux produce their pivot and/or rotation.

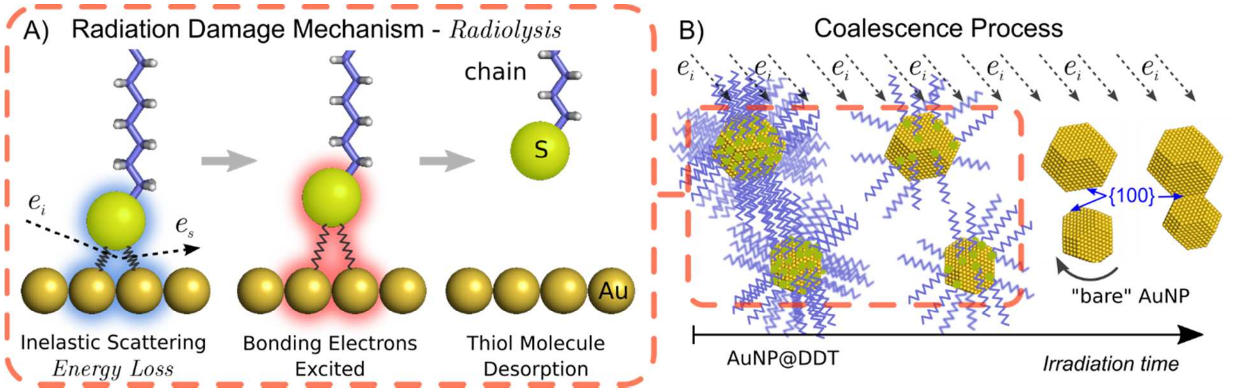

Scheme 1: (A) Radiolysis as the main radiation damage mechanism before the AuNPs coalescence. (B) RS desorption, followed by coalescence of AuNP@DDT under the electron beam in TEM. Compare with HRTEM images of Figure 3.

Further reasoning is needed to understand why only the {100} faces are involved in coalescence and ripening. On one side, the thiol (and/or Au_s-S-chain units) would be detached through radiolysis processes irrespective of the surface orientation ({100} or {111} faces). The thermodynamic driving force for crystal growth is the decrease in total energy. This decrease is the reason of the Ostwald ripening. For the oriented attachment observed in this study the same principle is applicable, neglecting entropy changes.[37] The surface energy of solids is related to their sublimation enthalpy. For FCC crystals, the surface energy ratio between faces {111} and {100} is $\gamma_{\{111\}}/\gamma_{\{100\}} \cong 0.87$ (see Supplementary Information). This means that {100} faces are more energetic than {111} faces, hence the coalescence across {100} faces is thermodynamically favored. On the other side, several early studies on Pt and Au NPs showed the atomic reconstruction of the {100} face.[7,16,28] This atomic reconstruction is a clear example about the higher surface energy of {100} faces.

Conclusion

This study explains the mechanism by which AuNP@SR are affected by the electron beam in the TEM. The radiation damage produces considerable sample modification when Au nanoparticles protected by alkanethiols are imaged in high-resolution TEM under standard operation conditions. The lack of understanding of the physical process involved during TEM characterization can lead to a wrong characterization of this kind of nanosystems. We observed that the particles can approach each other, and suffer coalescence and ripening as a consequence of their irradiation. Interestingly, these processes only occur between nearby particles when the {100} surfaces face each other, but they were not observed among other crystal orientations. Furthermore, the radiation damage does not depend on received doses but it does depend on crystal orientation.

The coalescence of thiol protected AuNPs only occur if their protecting monolayer is stripped of, which implies the thiol molecules desorption. The desorption of the thiol of {100} surfaces face seems to be the most probable scenario in order to maintain the stability of the coalesced particle. Otherwise, the number of total RS chains available of the two original particles would overcome the maximum calculated for the coalesced particles. Thes thiol desorption is probably the main effect of radiation damage during a characterization routine by TEM. The actual time needed to coalesce NPs is shorter than the time of damage calculated taking into account only knock-on radiation damage. For this reason, the main radiation process that favors the coalescence is radiolysis rather than knock-on. The radiolysis induces the RS desorption, at least, from the Au(100) surfaces. Otherwise, no coalescence would be observed. Furthermore, being the radiolysis the main source of radiation damage, partial or complete RS desorption is a probable scenario. In this context, the coalescence of the resulting naked AuNPs is more probable through the {100} faces due to their relative surface energy. The deep analysis of all of the probable irradiation damage mechanisms affecting a nanosystem gives another frame to the TEM characterization of this kind of materials. The nature of the radiation damage shows that the AuNPs behave more like as an insulating material than a conductor when irradiated in the TEM, which is interpreted as a size-effect.

The proper study of radiation damage of each sample is needed to arrive to confident interpretation of materials behavior.

ASSOCIATED CONTENT

Supporting Information. AuNPs size distribution, HRTEM images simulations, calculation about temperature increase, A listing of the contents of each file supplied as Supporting

AUTHOR INFORMATION

Corresponding Author

* E-mail: jcazcarate@cab.cnea.gov.ar (J.C.A.). Tel: +54-294-4445548. Fax: +54-294-4445299. Web: https://fisica.cab.cnea.gov.ar/metales

Author Contributions

The manuscript was written through contributions of all authors. All authors have given approval to the final version of the manuscript.

Funding Sources

The Consejo Nacional de Investigaciones Científicas y Técnicas (CONICET) PIP 0333, Universidad Naniocional de La Plata (UNLP), Comisión Nacional de Energía Atómica (CNEA) and Universidad Nacional de cuyo (UNCuyo) support this work.

Notes

The authors declare no competing financial interest.

ACKNOWLEDGMENT

The authors express their thanks to Adriano Geraci for the technical support and Dr. M.T. Malachevsky for his assistance in the manuscript edition.

REFERENCES

(1) Brust, M.; Walker, M.; Bethell, D.; Schiffrin, D. J.; Whyman, R. Synthesis of Thiol-Derivatised Gold Nanoparticles in a Two-Phase Liquid–Liquid System. *J. Chem. Soc., Chem. Commun.* **1994**, No. 7, 801–802.

(2) Hostetler, M. J.; Wingate, J. E.; Zhong, C.-J.; Harris, J. E.; Vachet, R. W.; Clark, M. R.; Londono, J. D.; Green, S. J.; Stokes, J. J.; Wignall, G. D.; et al. Alkanethiolate Gold Cluster Molecules with Core Diameters from 1.5 to 5.2 Nm: Core and Monolayer Properties as a Function of Core Size. *Langmuir* **1998**, *14*, 17–30.

(3) Azcárate, J. C.; Corthey, G.; Pensa, E.; Vericat, C.; Fonticelli, M. H.; Salvarezza, R. C.; Carro, P. Understanding the Surface Chemistry of Thiolate-Protected Metallic Nanoparticles. *J. Phys. Chem. Lett.* **2013**, *4*, 3127–3138.

(4) Corthey, G.; Giovanetti, L. J.; Ramallo-López, J. M.; Zelaya, E.; Rubert, A. A.; Benitez, G. A.; Requejo, F. G.; Fonticelli, M. H.; Salvarezza, R. C. Synthesis and Characterization of Gold@Gold(I)−Thiomalate Core@Shell Nanoparticles. *ACS Nano* **2010**, *4*, 3413–3421.

(5) Azcárate, J. C.; Floridia Addato, M. A.; Rubert, A.; Corthey, G.; Kürten Moreno, G. S.; Benítez, G.; Zelaya, E.; Salvarezza, R. C.; Fonticelli, M. H. Surface Chemistry of

Thiomalic Acid Adsorption on Planar Gold and Gold Nanoparticles. *Langmuir* **2014**, *30*, 1820–1826.

(6) Corthey, G.; Olmos-Asar, J. A.; Casillas, G.; Mariscal, M. M. M.; Mejía-Rosales, S.; Azcárate, J. C.; Larios, E.; José-Yacamán, M.; Salvarezza, R. C.; Fonticelli, M. H. Influence of Capping on the Atomistic Arrangement in Palladium Nanoparticles at Room Temperature. *J. Phys. Chem. C* **2014**, *118*, 24641–24647.

(7) Marks, L. D. Experimental Studies of Small Particle Structures. *Reports Prog. Phys.* **1999**, *57*, 603.

(8) Buffat, P. A. A. Electron Diffraction and HRTEM Studies of Multiply-Twinned Structures and Dynamical Events in Metal Nanoparticles: Facts and Artefacts. *Mater. Chem. Phys.* **2003**, *81*, 368–375.

(9) Barnard, S. S.; Lin, X. M.; Curtiss, L. A. Equilibrium Morphology of Face-Centered Cubic Gold Nanoparticles >3 Nm and the Shape Changes Induced by Temperature. *J. Phys. Chem. B* **2005**, *109*, 24465–24472.

(10) Wang, Z. W.; Palmer, R. E. Determination of the Ground-State Atomic Structures of Size-Selected Au Nanoclusters by Electron-Beam-Induced Transformation. *Phys. Rev. Lett.* **2012**, *108*, 245502.

(11) Marks, L. D.; Peng, L. Nanoparticle Shape, Thermodynamics and Kinetics. *J. Phys. Condens. Matter* **2016**, *28*, 53001.

(12) Olmos-Asar, J. A.; Ludueña, M.; Mariscal, M. M. Monolayer Protected Gold Nanoparticles: The Effect of the Headgroup–Au Interaction. *Phys. Chem. Chem. Phys.*

2014, *16*, 15979.

(13) Stenn, K.; Bahr, G. F. Specimen Damage Caused by the Beam of the Transmission Electron Microscope, a Correlative Reconsideration. *J. Ultrastruct. Res.* **1970**, *31*, 526–550.

(14) Egerton, R. F.; Li, P.; Malac, M. Radiation Damage in the TEM and SEM. *Micron* **2004**, *35*, 399–409.

(15) Bovin, J.-O.; Wallenberg, R.; Smith, D. J. Imaging of Atomic Clouds Outside the Surfaces of Gold Crystals by Electron Microscopy. *Nature* **1985**, *317*, 47–49.

(16) Wallenberg, L. R.; Bovin, J.-O.; Petford-Long, A. K.; Smith, D. J. Atomic-Resolution Study of Structural Rearrangements in Small Platinum Crystals. *Ultramicroscopy* **1986**, *20*, 71–75.

(17) Flüeli, M.; Buffat, P. A.; Borel, J.-P. Real Time Observation by High Resolution Electron Microscopy (HREM) of the Coalescence of Small Gold Particles in the Electron Beam. *Surf. Sci.* **1988**, *202*, 343–353.

(18) Surrey, A.; Pohl, D.; Schultz, L.; Rellinghaus, B. Quantitative Measurement of the Surface Self-Diffusion on Au Nanoparticles by Aberration-Corrected Transmission Electron Microscopy. *Nano Lett.* **2012**, *12*, 6071–6077.

(19) Gutiérrez-Wing, C.; Olmos-Asar, J. A.; Esparza, R.; Mariscal, M. M.; Yacamán, M. J. The Role of Ad-Atoms in the Coalescence of Alkanethiol-Passivated Gold Nanoparticles. *Electrochim. Acta* **2013**, *101*, 301–307.

(20) Yuk, J. M.; Jeong, M.; Kim, S. Y.; Seo, H. K.; Kim, J.; Lee, J. Y. In Situ Atomic Imaging

of Coalescence of Au Nanoparticles on Graphene: Rotation and Grain Boundary Migration. *Chem. Commun.* **2013**, *49*, 11479.

(21) Azcárate, J. C. Estudio Sobre La Modificación de Nanopartículas Metálicas Para El Desarrollo de Sensores Fluorescentes Fotomodulables, Universidad Nacional de La Plata, 2014.

(22) Stadelmann, P. The Java Electron Microscopy Software (JEMS). *Lausanne Interdiscip. Cent. Electron Microsc.* **2012**.

(23) Barragan, E. CPParticulas. *CPParticulas (GitHub)* **2016**, https://doi.org/10.5281/zenodo.572995. (accessed Oct 9, 2017)

(24) Smoluchowski, M. V. Drei Vortrage Uber Diffusion, Brownsche Bewegung Und Koagulation von Kolloidteilchen. *Zeitschrift fur Phys.* **1916**, *17*, 557–585.

(25) Marks, L. D.; Zhang, J. P. Is There an Electron Wind? *Ultramicroscopy* **1992**, *41*, 419–422.

(26) Olmos-Asar, J. a; Rapallo, A.; Mariscal, M. M. Development of a Semiempirical Potential for Simulations of Thiol-Gold Interfaces. Application to Thiol-Protected Gold Nanoparticles. *Phys. Chem. Chem. Phys.* **2011**, *13*, 6500–6506.

(27) Walter, M.; Akola, J.; Lopez-Acevedo, O.; Jadzinsky, P. D.; Calero, G.; Ackerson, C. J.; Whetten, R. L.; Grönbeck, H.; Häkkinen, H. A Unified View of Ligand-Protected Gold Clusters as Superatom Complexes. *Proc. Natl. Acad. Sci.* **2008**, *105*, 9157.

(28) Wallenberg, L. R.; Smith, D. J.; Petford-Long, A. K.; Wallenberg, L. R.; Bovin, J. O. Dynamic Atomic-Level Rearrangements in Small Gold Particles. *Science* **1986**, *233*, 872–

875.

(29) Casillas, G.; Velázquez-Salazar, J. J.; Jose-Yacaman, M. A New Mechanism of Stabilization of Large Decahedral Nanoparticles. *J. Phys. Chem. C* **2012**, *116*, 8844–8848.

(30) Hobbs, L. W. Radiation Effects in Analysis of Inorganic Specimens by TEM. In *Introduction to Analytical Electron Microscopy*; Hren, J. J., Goldstein, J. I., Joy, D. C., Eds.; Springer US: Boston, MA, 1979; pp 437–480.

(31) Egerton, R. F.; McLeod, R.; Wang, F.; Malac, M. Basic Questions Related to Electron-Induced Sputtering in the TEM. *Ultramicroscopy* **2010**, *110*, 991–997.

(32) Egerton, R. F. Mechanisms of Radiation Damage in Beam-Sensitive Specimens, for TEM Accelerating Voltages Between 10 and 300 kV. *Microsc. Res. Tech.* **2012**, *75*, 1550–1556.

(33) Reimers, J. R.; Ford, M. J.; Halder, A.; Ulstrup, J.; Hush, N. S. Gold Surfaces and Nanoparticles Are Protected by Au(0)–thiyl Species and Are Destroyed When Au(I)–thiolates Form. *Proc. Natl. Acad. Sci.* **2016**, *113*, E1424–E1433.

(34) Mariscal, M. M.; Olmos-Asar, J. A.; Gutierrez-Wing, C.; Mayoral, A.; Yacaman, M. J. On the Atomic Structure of Thiol-Protected Gold Nanoparticles: A Combined Experimental and Theoretical Study. *Phys. Chem. Chem. Phys.* **2010**, *12*, 11785–11790.

(35) Hu, G.; Jin, R.; Jiang, D. Beyond the Staple Motif: A New Order at the Thiolate–gold Interface. *Nanoscale* **2016**, *8*, 20103–20110.

(36) Lide, D. R. *CRC Handbook of Chemistry and Physics, 85th Edition*; CRC Handbook of Chemistry and Physics, 85th Ed; Taylor & Francis, 2004.

(37) Zhang, H.; Banfield, J. F. Energy Calculations Predict Nanoparticle Attachment Orientations and Asymmetric Crystal Formation. *J. Phys. Chem. Lett.* **2012**, *3*, 2882–2886.

TOC graphic

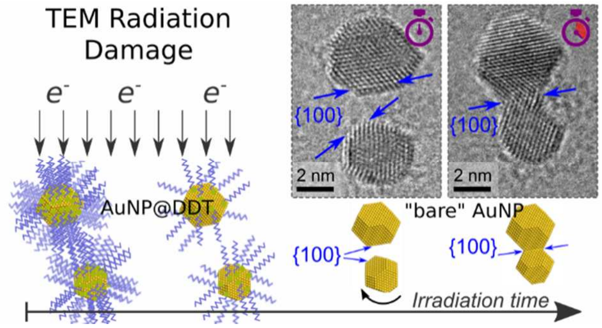
TEM Radiation Damage
e⁻
e⁻
e⁻
AuNP@DDT
{100}
2 nm
{100}
2 nm
"bare" AuNP
{100}
{100}
Irradiation time

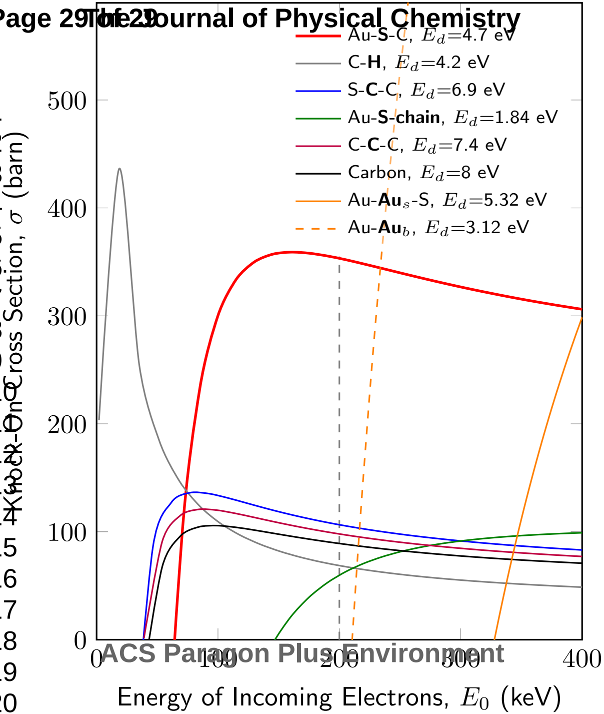
Au-**S**-C, E_d=4.7 eV
C-**H**, E_d=4.2 eV
S-**C**-C, E_d=6.9 eV
Au-**S-chain**, E_d=1.84 eV
C-**C**-C, E_d=7.4 eV
Carbon, E_d=8 eV
Au-**Au**$_s$-S, E_d=5.32 eV
Au-**Au**$_b$, E_d=3.12 eV
Knock-On Cross Section, σ (barn)
0
100
200
300
400
500
0
100
200
300
400
Energy of Incoming Electrons, E_0 (keV)